Available online at www.sciencedirect.com
SCIENCE DIRECT®
Biomaterials 25 (2004) 5171–5180
Biomaterials
www.elsevier.com/locate/biomaterials

Biphasic calcium phosphate nanocomposite porous scaffolds for load-bearing bone tissue engineering

Hassna R.R. Ramay, M. Zhang*

University of Washington, Seattle, WA, USA

Received 21 September 2003; accepted 8 December 2003

Abstract

A novel biodegradable nanocomposite porous scaffold comprising a β-tricalcium phosphate (β-TCP) matrix and hydroxyl apatite (HA) nanofibers was developed and studied for load-bearing bone tissue engineering. HA nanofibers were prepared with a biomimetic precipitation method. The composite scaffolds were fabricated by a method combining the gel casting and polymer sponge techniques. The role of HA nanofibers in enhancing the mechanical properties of the scaffold was investigated. Compression tests were performed to measure the compressive strength, modulus and toughness of the porous scaffolds. The identification and morphology of HA nanofibers were determined by X-ray diffraction and transmission electron microscopy, respectively. Scanning electron microscopy was used to examine the morphology of porous scaffolds and fracture surfaces to reveal the dominant toughening mechanisms. The results showed that the mechanical property of the scaffold was significantly enhanced by the inclusion of HA nanofibers. The porous composite scaffold attained a compressive strength of 9.8 ± 0.3 MPa, comparable to the high-end value (2–10 MPa) of cancellous bone. The toughness of the scaffold increased from 1.00 ± 0.04 to 1.72 ± 0.02 kN/m, as the concentration of HA nanofibers increased from 0 to 5 wt %.

Keywords: Porous scaffolds; Nanofibers; Bone; Tissue engineering

1. Introduction

Over the past 20 years, there has been great interest in use of calcium phosphates, a principal inorganic constituent of natural bone, as scaffolding materials for bone tissue engineering [1–5]. Different phases of calcium phosphates were employed to fabricate porous scaffolds to accommodate bone tissue regeneration in vitro or in vivo. The atomic ratio of Ca/P in calcium phosphates can be varied between 1.5 and 2 to produce compounds ranged from calcium tetraphosphate ($Ca_4P_2O_9$), hydroxyapatite (HA) $Ca_{10}(PO_4)_6(OH_2)$ to tricalcium phosphate (TCP) $Ca_3(PO_4)_2$. The degradability of calcium phosphates generally varies with the Ca/P ratio, with the highest being of TCP that usually results in the most extensive bone remodeling around the scaffold [6–9]. Among these bioceramics, HA and β-tricalcium phosphate (β-TCP) are most widely used. They allow osteogenesis to occur and form tight bonds with host bone tissues [10,11]. Recently, there is a growing interest in developing HA/β-TCP biphasic calcium phosphate (BCP) ceramics as scaffolding materials because they are more effective in bone repair or regeneration than pure HA or pure β-TCP, and have a controllable degradation rate to a certain degree [12–17].

In addition to compositional requirements, scaffolds for bone tissue engineering must also have a porous structure [18,19]. A porous structure promotes cell attachment, proliferation, and differentiation, and provides pathways for biofluids. Consequently, a high porosity, interconnected pore structure generally favors tissue regeneration. However, a material generally weakens as its porosity increases, which poses a major challenge in developing load-bearing scaffolds. Because of their natural brittleness, ceramics such as HA and β-TCP, in a porous form, have very low strength and toughness. Thus, despite their favorable biological properties, the poor mechanical properties of these ceramic materials have severely hindered their clinical applications [20,21].

Theoretical and experimental investigations for use of disperse particulate inclusions to strengthen or toughen dense materials have been actively pursued during the past few years, largely because of our increased capability

*Corresponding author.
E-mail address: mzhang@u.washington.edu (M. Zhang).

0142-9612/$ - see front matter © 2003 Elsevier Ltd. All rights reserved.
doi:10.1016/j.biomaterials.2003.12.023

of producing micro- and nano-scale crystals (particles, rods, or fibers) in a controlled manner (for size, shape, and crystalline structure) [22–26]. This strategy has proved to be quite successful for dense materials, but little is known about its effectiveness for porous structures. Although the studies reported up to date have focused on dense materials for constructional, optical, electrical or electronic applications, theoretically, the principle can be applied equally well to porous biomaterials, provided that the pore wall thickness of the porous scaffolds is much greater than the particle size. As shown in previous work by the authors and other investigators [27–29], porous scaffolds for tissue engineering typically have wall thickness of a few microns. To this end, particulates in the nanoscale are suitable candidates to serve as the particulate inclusion in the porous structure.

In our recent work [27], we introduced a polymer-gel method to prepare porous HA scaffolds that can attain a compressive modulus of 5 MPa, a quantity comparable to human cancellous bone (2–10 MPa) [30]. Based on this method, this research seeks to further increase the mechanical strength and toughness of the scaffolds by inclusion of a second phase of nanofibers (HA) in a porous bioceramic matrix (β-TCP) to prepare a nanocomposite scaffold and to study the mechanism involved in this enhancement. β-TCP is chemically stable and has a fairly fast bioresorption rate [31], while HA degrades slowly in vivo and may take years to be resorbed [10,15,32]. Accordingly, a biphasic porous composite of β-TCP and HA can be tailored by controlling contents of HA and β-TCP to achieve desired biodegradation rate [12,33]. Due to diminutive amount of particulate inclusion, nanofibers made of HA can be easily resorbed in vivo [34]. HA nanofibers were prepared using a biomimetic precipitation method. The porous β-TCP scaffolds were prepared with a procedure similar to that reported previously [27], with additionally incorporating HA nanofibers of various amount. Compressive strength and modulus of porous scaffolds were measured with an Instron mechanical tester. The toughness of the scaffolds was calculated using the area of stress displacement curve obtained from the compression tests. Scanning electron microscopy (SEM) was used to characterize the porous structure and fracture behavior of the composite scaffolds. The chemical composition and phase characterization before and after sintering were determined by X-ray diffraction (XRD). The sintering behavior of β-TCP with different HA concentrations was evaluated with a dilatometer.

2. Experimental procedure

2.1. Materials

β-TCP (β-$Ca_3(PO_4)_2$) powder was used as received. Darvan C (Vanderbilt Company Inc.), a 25% aqueous solution of ammonium polymethacrylate, was used as a dispersant. Monofunctional acrylamide $C_2H_3CONH_2$ difunctional methylenebisacrylamide$(C_2H_3CONH)_2CH_2$ were used in the gel-casting process as the monomers and ammonium persulphate $(NH_4)_2S_2O_8$ and N,N,N',N' tetramethylethylenediamine (TEMED) as the initiator and catalyst, respectively. All these chemicals were purchased from Sigma-Aldrich Corporation. A silicone based defoamer, Surfonal® DF 58 (Air Products and Chemicals), was used as a surfactant. All the slurries were aqueous. De-ionized (DI) water was used in all the experiments. Hydroxyapatite nanofibers (HA nanofibers) were prepared with calcium nitrate tetrahydrate $(Ca(NO_3)_2 \cdot 4H_2O)$ and ammonium hydrogen phosphate $((NH_4)_2PO_4)$, obtained from Sigma-Aldrich Corporation. Polypropylene glycol $(H[OCH(CH_3)CH_2]_nOH)$, used to disperse HA fibers, was obtained from Alfa Aesar Corporation.

2.2. Synthesis of HA nanofibers

HA nanofibers were prepared via a chemical precipitation process via chemical reaction:

$$10Ca(NO_3)_2 + 6(NH_4)_2HPO_4 + 8NH_4OH \rightarrow Ca_{10}(PO_4)_6(OH)_2 + 6H_2O + 20NH_4NO_3$$

In all 19.75 g of $(NH_4)_2PO_4$ were added to DI water to make a 400 ml solution of diammonium hydrogen phosphate. A total of 300 ml calcium nitrate solution was prepared by dissolving 57.5 g of $Ca(NO_3)_2 \cdot 4H_2O$ in DI water. The pH of the solution was adjusted to 10.4 by addition of NH_4OH. White precipitates of hydroxyapatite were formed by adding the diammonium hydrogen phosphate solution into the calcium nitrate solution at a rate of 1.5 ml/min under constant stirring. The white precipitates were aged for 100 h to form HA nanofibers. The nanofibers washed with DI water until the pH value decreased to 7. The water surrounding the HA nanofibers was then replaced with 1-butanol to prevent the HA nanofibers from aggregation during the drying process. The precipitates were dried at 80°C and calcined at 400°C to remove the rudimental organic compound.

2.3. Nanocomposite scaffolds

β-TCP/HA scaffolds were prepared through a gel-polymer process that integrates the gel casting and polymer sponge methods [27]. HA fibers of 0, 1, 2, 3, 4 and 5 wt % were mixed with β-TCP powder, along with monomers (acrylamide, methylenebisacrylamde), dispersant (Darvan C) and surfactant (Surfonal®), to make ceramic slurries with 75 wt % solid loading. The slurries prepared were deagglomerated by ball milling for 24 h and subsequently de-aired under a vacuum environment until no further release of air bubbles from

the slurries. Catalyst (ammonium presulphate) and initiator (N,N,N',N' tetramethylethylenediamine) were added to the slurries to polymerize the monomers. To prepare porous scaffolds, polyurethane foam cut into desired shapes and sizes was immersed into the slurries under vacuum to force the ceramic slurries into the pores of the foam. The samples were placed in a nitrogen chamber during the polymerization to avoid oxygen contamination, which may inhibit the polymerization process. The polymerized samples were dried in air for 24 h and heated at a rate of 1°C/min to 600°C. The samples remained at this temperature for 1 h to burn out the polyurethane foams, and then were sintered with temperature increased at a rate of 3°C/min to the sintering temperature for a dwell time of 1 h. The sintering temperature, which depends on the HA nanofiber content in the scaffold, was evaluated with a dilatometer.

2.4. X-ray diffraction analysis

X-ray diffraction (XRD) was used to characterize the crystallinity, chemical composition, and structure of the materials. XRD experiments were performed on HA nanofibers and biphasic calcium phosphate (BCP) ceramics before and after sintering, with a Phillips X'Pert using CuKα radiation at 20 mA, 40 kV. Scans were performed with 2θ values from 20° to 40° at a rate of 0.2°/min.

2.5. Transmission electron microscopy (TEM)

The morphology of HA nanofibers was observed with a transmission electron microscope (CM 100 TEM) at an accelerating voltage of 100 kV. Samples were prepared by drying the solution of HA nanofibers on a copper grid, fitted with a carbon support film, under vacuum. The solution was prepared by dispersing 0.05 g of HA nanofibers in 0.5 vol% polypropylene glycol under sonication (550 Sonic Dismembrator, Fisher Scientific, Pittsburgh, PA).

2.6. Dilatometery

The sintering temperature of BCP was determined with a Netzsch Dilatometer. Samples were heated in Netzsch tube furnace from 20°C to 1400°C at a rate of 3°C/min.

2.7. Scanning electronic microscopy (SEM)

Morphology of porous composites was studied with a JEOL 5200 scanning electron microscope. The samples were pre-coated with gold/palladium under an argon atmosphere.

2.8. Mechanical testing

The specimens of porous scaffolds were cylindrical (2 mm height × 1 mm diameter) in shape with a length to diameter ratio of 2:1. An Instron 4505 mechanical tester with 10 kN load cells was used for the compression mechanical tests. The crosshead speed was set at 0.4 mm/min, and the load was applied until the scaffold was crushed completely. The elastic modulus was calculated as the slope of the initial linear portion of the stress-strain curve. The yield strength was determined from the cross point of the two tangents on the stress-strain curve at the maximum stress [35]. The toughness was calculated from the area under the stress displacement curve from zero to the point where the final densification starts [36]. Five samples of each type were tested for mechanical properties.

3. Results and discussion

In a recent work, we introduced a processing technique for fabrication of porous HA scaffolds for bone tissue engineering [27]. The technique incorporates the gel casting technique with polymer sponge method, and can produce interconnected porous scaffolds with high compressive modulus and strength. The scaffolds made of HA have a slow degradation rate [37–40], while β-TCP, serving as the matrix material in this study, is bioresorbable and has a fairly fast degradation rate [37–39]. Research showed that biphasic calcium phosphate (BCP) scaffolds, can lead to fast bone formation for bone reconstruction. BCP implants have been shown to be surrounded by new bone tissues within a few weeks after implantation at bony sites [15,16,41,42].

Addition of a nanoparticulate second phase to a solid ceramic matrix is known as a method of achieving enhanced mechanical strength and toughness of the matrix. The conformation of a particulate second phase in a ceramic matrix can be broadly grouped into three types [43]: (a) intergranular, (b) transgranular, and (c) particulate/particulate as illustrated in Fig. 1, depending on whether the particulate phase is located within matrix grains, at boundaries of grains, or simply is part of the matrix. Two mechanisms for toughness enhancement are widely accepted [44]. In the first mechanism, the nanoparticles serve to steer cracks to propagate along the paths of higher toughness. The toughness at grain boundaries is lower than within grains. The internal stress produced by the nanoparticles at grain boundaries tends to alter the crack propagation path from intergranular to transgranular, and thus increases the overall toughness of the material. In the second mechanism, the gross toughening is achieved by local weakening. The local residual stresses generated by the particulate phase promote crack curving in ceramic

matrices, and thus the crack propagates along a wavy path. Apart from imparting high toughness, particulates inclusion in a ceramic matrix also increases the strength of the matrix [45,46]. Further, nanoparticles will also improve sinterability and reduce flaw size [47,48].

In the present study, hydroxyapatite nanofibers were prepared via a wet chemical process that can control the fiber size, shape and composition. The pH of the solution, and aging temperature and time can affect the size and morphology of resultant nanofibers. Fig. 2 shows a TEM image of synthesized HA nanofibers. It is seen that the fibers are well dispersed with uniform morphology and a dimension of $\sim$100 nm in length and $\sim$20 nm in diameter. These HA nanofibers were aged for 100 h, yielding a well-crystallized structure. The aging process ensured that the reagents were fully reacted and precipitated. The prolonged aging time reduced crystal strains in the matrix and recrystallized non-homogeneous grains to generate more homogeneous grains [49]. In Fig. 3, the XRD pattern of the HA nanofibers is compared with the diffraction pattern of standard crystalline HA (Card No. 9-432). The peak locations for the HA nanofibers are seen to agree well with those of standard crystalline HA. The peak broadening in the diffraction pattern is the result of size reduction associated with the nanoscaled HA fibers [50].

The inter/trans granular (Fig. 1) type of nanocomposite scaffolds were prepared with β-TCP as the matrices and HA fibers as the particulate inclusion by a gel-polymer method that integrates the gel casting technique with polymer sponge method. The scaffolds were prepared with six different HA concentration: 0, 1, 2, 3, 4 and 5 wt%. Polymer removal and sintering were carried out in a single heating cycle. The polymer was carefully removed to minimize the component distortion and internal defects. Incomplete polymer removal can result in carbon retention, which has been shown to impede sintering [51,52]. Heating temperature can be controlled to minimize component distortion through the use of slow heating rates and low dwell temperature [53]. This allows for more uniform heating so that the material can be removed at a controlled rate throughout the entire sample rather than localized zones. The sintering cycle for the ceramic scaffolds combined a low temperature dwell at 600°C with a slow heating rate of 1°/min. Sintering calcium phosphates at high temperature may lead to the formation of decomposition products, which can impair the densification and biological response of the scaffold [31,42]. To prevent the second phase from decomposition at high tempera-

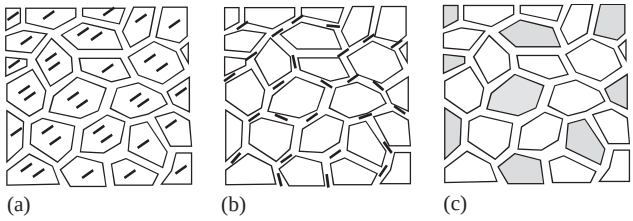

Fig. 1. A schematic of types of nanocomposites: (a) intergranular, (b) transgranular and (c) nano/nanocomposite.

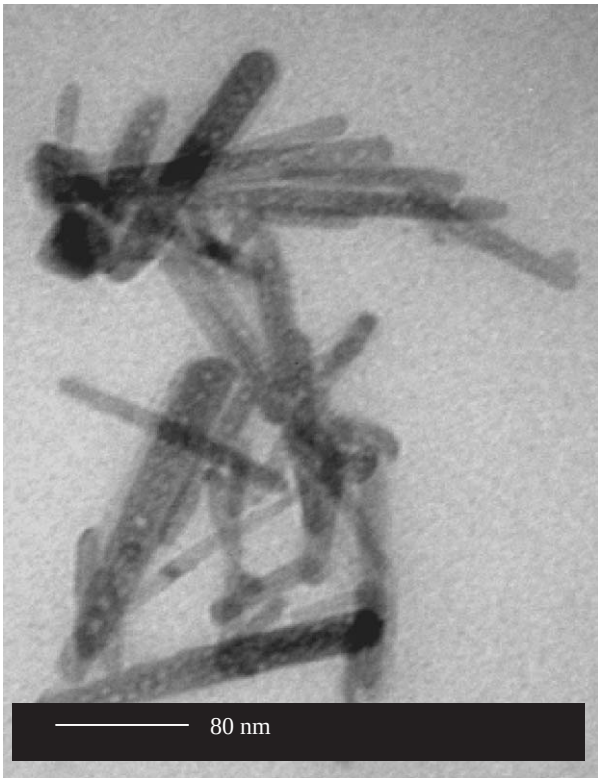

Fig. 2. TEM micrograph of hydroxyapatite nanofibers prepared by a biomimetic method.

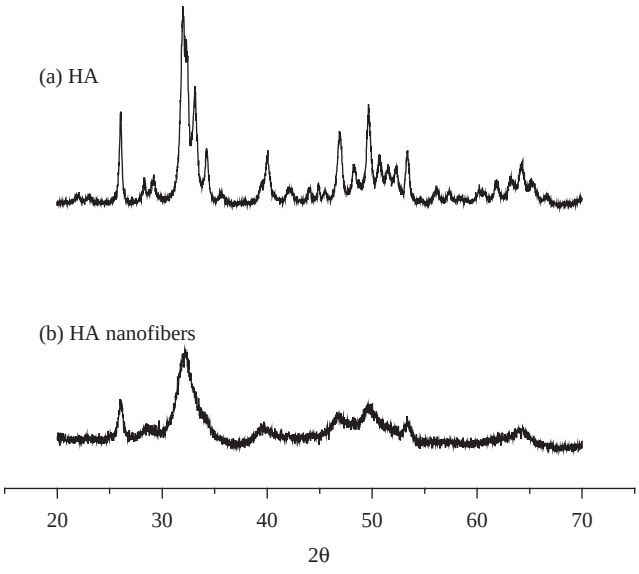

Fig. 3. XRD spectra of (a) standard HA powder and (b) HA nanofibers.

ture, the precise sintering temperature must be determined for the nanocomposite material. This was done with a dilatometer. A dilatometer measures the length change of a sample as a function of temperature. The sintering temperature is established from the point of the maximum sample shrinkage, i.e., the maximum density that can be achieved for the sample. Dilatometric studies have also been employed by other investigators to determine sintering temperature [54,55].

During continuous heating of a sample with a dilatometer, the change in the length (dL) and temperature (T) as a function of time were recorded. Fig. 4 shows the relations of dL vs. heating temperature for the BCP samples with 0 and 5 wt% of HA nanofibers incorporated, tested at a temperature increasing rate of 3°C/min. The sintering temperature, at which the samples attained their minimum change in length dL, is marked with arrows in Fig. 4. The sintering temperature for pure β-TCP is 1274°C, and drops to 1144°C for the sample with 5 wt% of HA nanofibers incorporated. The addition of nanofibers reduces the sintering temperature of the ceramic matrix, a phenomenon attributed to their high surface reactivity [47]. A lower sintering temperature is favored because it can reduce the cost of material processing and prevent the second phase decomposition which often occurs at high temperature and deteriorates the biological and mechanical properties of biomaterials [56,57].

TCP has three polymorphs, β-TCP, α-TCP and α'-TCP. Among these polymorphs, β-TCP is preferred, and thus was chosen, as a bioceramic in this study, because of its chemical stability, relatively high mechanical strength, and favorable bioresorption rate [58]. The mechanical properties of β-TCP depend in part on its density, which can be optimized by sintering process. Generally, it is difficult to achieve a pure phase of sintered β-TCP because β-TCP progressively transforms to α-TCP when sintered above 1300°C [59,60]. Fig. 5 shows the X-ray diffraction patterns of the β-TCP samples with different concentrations of HA nanofibers before and after sintering. All the samples show only characteristic peaks of β-TCP (JCPDS 9-169 and JCPDS 9-432), suggesting that β-TCP phase did not change into other phases during the sintering. This is important for achieving good mechanical and biological properties of produced scaffolds. The HA peaks are not discernible in the diffraction patterns because of low HA content in the samples [50].

The porosity of the sintered BCP scaffolds, as measured with the Archimedes method in distilled water, is $\sim 73 \pm 0.4\%$. Fig. 6 shows the porous structure of a scaffold as seen with a scanning electron microscope (SEM). The SEM image also reveals the interconnected macroporous structure of the scaffold with a pore size ranged in 300–400 μm. The sample size (diameter = 1 mm) to pore size ratio is $\sim 1000/3$. The macroporous structure is necessary for cell growth and vascularization [18,61]. Fig. 7 shows pore wall microstructure of a sintered biphasic nanocomposite scaffold in two different (a, b) magnifications. The highly densified pore walls were resulted from high solid loading and accurate control of sintering time and temperature. HA concentrations higher than 5 wt% would yield a high viscous slurry that cannot be dispersed and gel-casted. The high solid loading (75 wt%) was achieved by proper use of homogenous deflocculants.

One of the major challenges in developing load-bearing scaffolds for bone tissue engineering is the conflicting interest between material porosity and

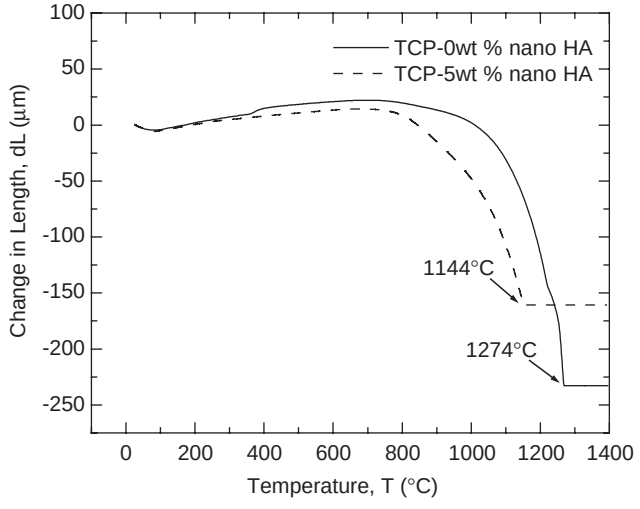

Fig. 4. Change in length vs. temperature for biphasic (TCP-HA) nanocomposite at two different weight compositions.

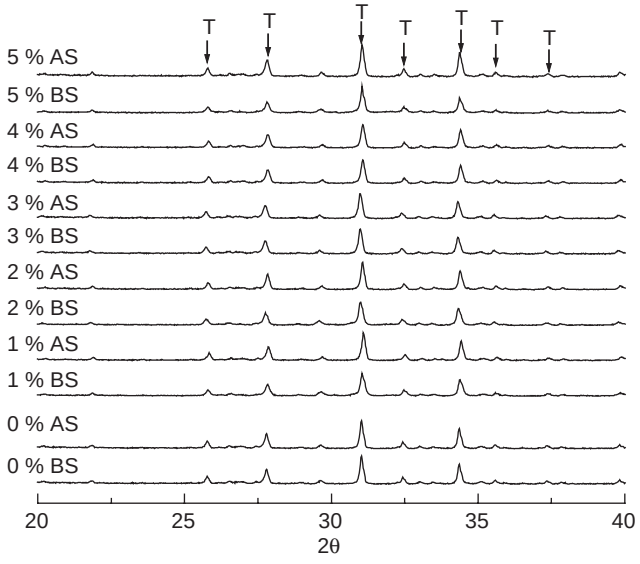

Fig. 5. X-ray diffraction patterns for nanocomposite, containing different percentages (%) of nano hydroxyapatite in tricalcium phosphate, before (BS) and after (AS) sintering. T represents the X-ray peaks for β -TCP.

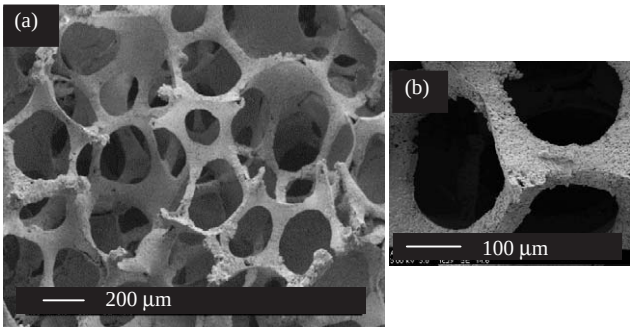

Fig. 6. SEM micrograph of porous biphasic (TCP-HA) nanocomposite, showing (a) porous structure and (b) pore wall.

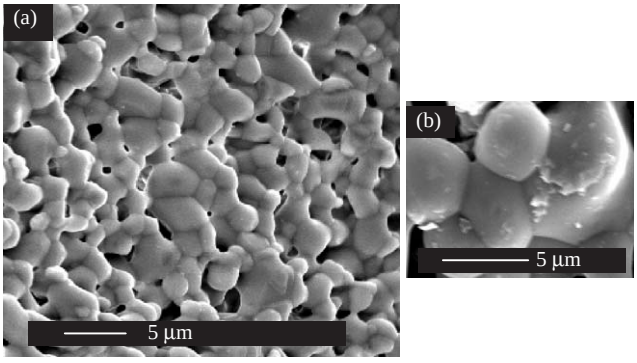

Fig. 7. SEM micrograph of sintered pore wall of biphasic (TCP-HA) nanocomposite scaffold at two different (a, b) magnifications.

mechanical strength. A highly porous structure is preferred in favor of cell growth and proliferation, but achieved at the expense of mechanical strength. Although there is no clearly defined criterion in mechanical properties required by bone tissue engineering, it is generally accepted that the scaffolding material should have mechanical strength as close as possible to the strength of the bone to be repaired or substituted. In this study, β-TCP ceramic matrices were reinforced and toughened by incorporating HA nanofibers and by adjusting processing conditions to achieve a highly densified porous structure.

Compression tests were performed to characterize the mechanical properties of the prepared scaffolds. The specimens were made cylindrical in shape with a length to diameter ratio of 2:1, which was designed to minimize the end effect imposed by compressive loading [62]. The compressive strength and elastic modules were determined from the stress–strain relations obtained. Fig. 8 shows the compressive strength and elastic modulus of the porous BCP scaffolds, respectively, as a function of HA fiber concentration in the scaffolds. Both the compressive strength and modulus are seen to increase with the increase of HA fiber concentration. HA nanofibers can easily diffuse to the grain boundaries of the BCP matrix during sintering due to their high

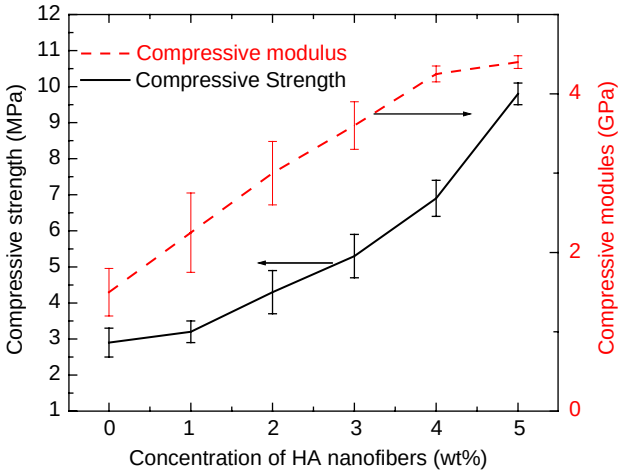

Fig. 8. Compressive strength and modulus of porous nanocomposite scaffolds as function of concentration of HA nanofibers.

surface energy. The high diffusion rate resulting from high surface energy gives rise to better inter particle contact and increases the elastic modulus of the scaffold [63]. The scaffold containing 5 wt% HA nanofibers attained a compressive strength of 9.8 ± 0.3 MPa, which is comparable to the high end of compressive strength of cancellous bone (2–10 MPa) [30].

Fracture toughness, the material's resistivity to crack propagation, is an important parameter to assess the susceptibility of a scaffold to failure. Fig. 9 (a) shows the typical stress strain curve from compression testing. The toughness was calculated from the area under the stress displacement curve from zero to the point where the final densification starts (region C in Fig. 9 (a)) [36]. Five samples of each type were tested for mechanical properties. Fig. 9 (b) shows the change in toughness of BCP scaffolds as a function of HA fiber concentration in the scaffolds. The toughness is seen to increase from 1.00 ± 0.04 to 1.72 ± 0.02 kN/m as the concentration of HA fibers increased from 0 to 5 wt%. The fracture surfaces obtained from the compressive tests were characterized by SEM. Fig. 10 shows the fractured pore wall structures of BCP scaffolds with different wt% of HA nanofibers. The fracture mode is seen to change from intergranular to more and more transgranular as the concentration of HA nanofibers increased from 0 to 5 wt%. The transgranular mode of fracture reveals a strong grain boundary effect on toughness [64,65]. Grain boundary effect might be due to the residual stresses associated with different coefficients of thermal expansion [66,67] of HA (13.7×10^{-6} °C) and β-TCP (14.85×10^{-6} °C) [68] or the compressive residual stresses associated with the particulate inclusions, leading to crack pinning [69,70]. The HA nanofibers residing at and pinning the crack front might also effectively cause crack bridging due to stresses associated with the particulate inclusions [69]. The interac-

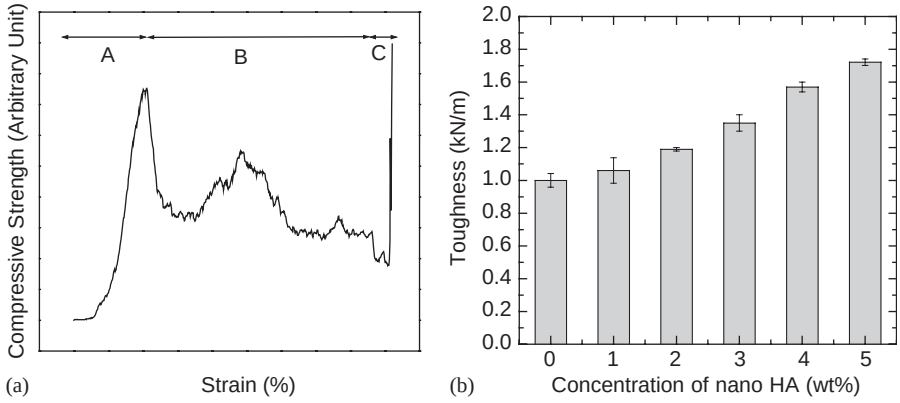

Fig. 9. (a) A schematic of the stress strain curve obtained from compression testing of TCP-HA nanocomposite, showing different regions of strain characteristics of an elastic brittle foam. (b) Toughness of porous nanocomposite scaffolds as function of concentration of HA nanofibers.

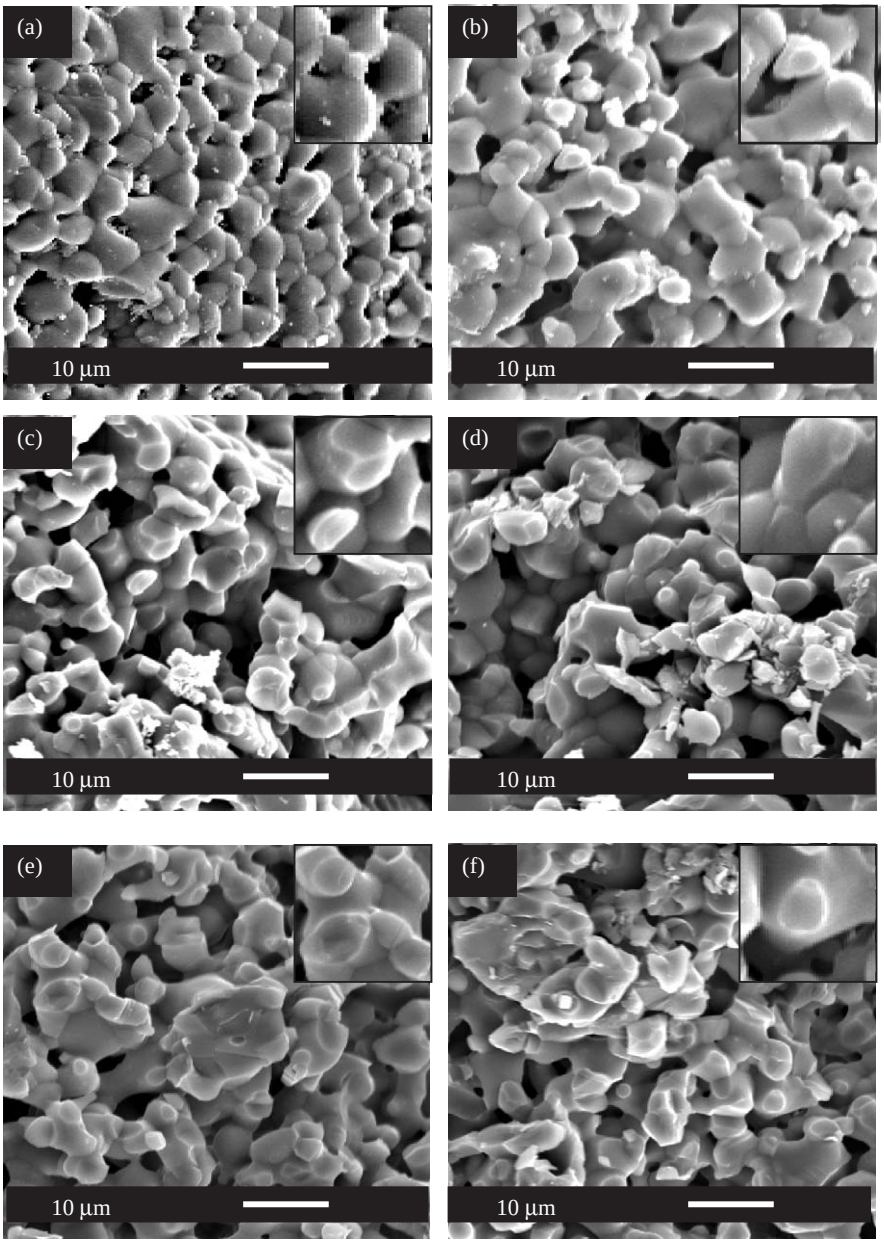

Fig. 10. SEM micrographs of fractured surface of porous biphasic (TCP-HA) nanocomposite scaffold with (a) 0, (b) 1, (c) 2, (d) 3, (e) 4 and (f) 5 wt% HA nanofibers.

tions of cracks in the nanocomposites with stress fields around HA nanofibers promoted crack propagation in the ceramic matrix along a wavy path [71,72]. Thus, the transgranular fracture is observed as a result of both matrix weakening and grain boundary strengthening. This suggests that both toughening mechanisms described above may contribute to the toughness enhancement.

4. Conclusions

The concept of nanocomposites has been introduced for the first time to porous scaffolds for bone tissue engineering. Nanocomposites made of β-TCP as a matrix and HA nanofibers of different concentrations have been used to fabricate porous scaffolds through a technique that integrating the gel casting with polymer sponge methods. The experimental results showed that inclusion of HA nanofibers as a second phase in β-TCP porous ceramic matrix significantly improved the mechanical properties of the porous scaffold. The porous scaffold with a porosity of $\sim 73\%$ and containing 5 wt% HA nanofibers attained a compressive strength of 9.8 ± 0.3 MPa, which is comparable to the high end value of cancellous bone. The toughness of BCP ceramics was 1.72 ± 0.02 kN/m with 5 wt% nano HA fibers incorporated. These porous scaffolds reinforced with nanofibers have better mechanical properties than the scaffolds of single-phase calcium phosphate prepared previously.

Bone tissue engineering is a promising approach for treatment of defective and lost bone. Fabrication of biodegradable and osteoconductive scaffolds with a 3D interconnected porous structure and adequate mechanical strength and toughness has been a formidable challenge. This study promises a new class of porous scaffolds as a cost-effective therapy for load bearing bone reconstruction.

Acknowledgements

The authors would like to thank the University Of Washington Engineered Biomaterials Research Center for partial financial support (NSF-EEC 9529161), Dr. Brian Flinn for his suggestions, and Mr. Enoch Shum for his lab assistance.

References

[1] LeGeros RZ. Properties of osteoconductive biomaterials: calcium phosphates. Clin Orthop Rel Res 2002;395:81–95.
[2] De Groot K. Macroporous tissue ingrowth: a quantitative and qualitative study on hydroxyapatite ceramics. Biomaterials 1986;7:137–43.
[3] Jarcho M. Biological aspects of calcium phosphates: properties and applications. Dent Clin North Am 1986;30:25–47.
[4] Bucholz RW, Carlton A, Holmes FE. Hydroxyapatite and tricalcium phosphate bone graft substitutes. Orthop Clin North Am 1987;18:323–34.
[5] Hench LL. Bioceramics. J Am Ceram Soc 1998;81:1705–28.
[6] Klein CPAT, de Blieck-Hogervorst JMA, Wolke JGC, de Groot K. Studies of the solubility of different calcium phosphate ceramic particles in vitro. Biomaterials 1990;11:509–12.
[7] Tas AC, Korkusuz F, Timucin M, Akkas N. An investigation of the chemical synthesis and high temperature sintering behavior of calcium hydroxyapatite (HA) and tricalcium phosphate (TCP) bioceramics. J Mater Sci Mater Med 1997;8:91–6.
[8] Jarcho M. Calcium phosphate ceramics as hard tissue prosthetics. Clin Orthop Rel Res 1981;157:259–78.
[9] Klein CPAT, Driessen AA, de Groot K. Relationship between the degradation behavior of calcium phosphate ceramics and their physical chemical characteristics and ultra structural geometry. Biomaterials 1984;5:157–60.
[10] Ducheyne P, de Groot K. In vivo surface activity of a hydroxyapatite alveolar bone substitute. J Biomed Mater Res 1981;15:441–5.
[11] Aoki H. Medical applications of hydroxyapatite. St. Louis: Ishiyaku Euro America; 1994: p. 13–74.
[12] Kwon SH, Jun YK, Hong SH, Kim HE. Synthesis and dissolution behavior of β-TCP and HA/β-TCP composite powders. J Eur Ceram Soc 2003;23:1039–45.
[13] Harada Y. Experimental studies of healing process on compound blocks of hydroxyapatite particles and tricalcium phosphate powder implantation in rabbit mandible. J Tokyo Dent College Soc 1989;89:263–97.
[14] Ryu HS, Yuoun HJ, Hong KS, Chang BS, Lee CK, Chung SS. An improvement in sintering property of β-Tricalcium phosphate by addition of calcium pyrophosphate. Biomaterials 2002;23:909–14.
[15] Kohri M, Miki K, Waite DE, Nakajima H, Okabe T. In vivo stability of biphasic calcium phosphate ceramics. Biomaterials 1993;14:299–304.
[16] Nery EB, LeGeros RZ, Lynch KL, Lee K. Tissue response to biphasic calcium phosphate ceramic with different ratios of HA/βTCP in periodontal osseous defects. J Periodontal 1992;63:729–35.
[17] Wang J, Chen W, Li Y, Fan S, Weng Jie, Zhang X. Biological evaluation of biphasic calcium phosphate ceramic vertebral laminae. Biomaterials 1998;19:1387–92.
[18] Hing KA, Best SM, Bonefield W. Characterization of porous hydroxyapatite. J Mater Sci Mater Med 1999;10:135–45.
[19] De Oliverira JF, De Aguiar PF, Rossi AM, Soares GA. Effect of process parameters on the characteristics of porous calcium phosphate ceramics for bone tissue scaffolds. Int Soc Art Org 2003;27:406–11.
[20] Ducheyne P. Bioceramics: material characteristics versus in vivo behavior. J Biomed Mater Res 1987;21:219–36.
[21] Yaszemski MJ, Payne RF, Hayes WC, Lander R, Mikos AG. Evolution of bone transplantation: molecular, cellular and tissue strategies to engineer human bone. Biomaterials 1996;17:175–85.
[22] Greil P. Advanced engineering ceramics. Adv Mater 2002;14:709–16.
[23] Wahi RP, Ilschner B. Fracture behavior of composites based on Al_2O_3–TiC. J Mater Sci 1980;15:875–85.
[24] Claussen N. Strengthening strategies for ZrO_2 toughened ceramics at high temperatures. Mater Sci Eng 1984;71:23–8.

[25] Lange FF. Effect of microstructure on strength of Si_3N_4–SiC composite system. J Am Ceram Soc 1973;56:445–50.
[26] Zhu YT, Beyerlein IJ. Bone shaped short fiber composites-an overview. Mater Sci Eng 2002;A236:208–27.
[27] Ramay HR, Zhang M. Preparation of porous hydroxyapatite scaffolds by combination of the gel casting and polymer sponge methods. Biomaterial 2003;24:3292–302.
[28] Zhang Y, Zhang M. Three dimensional macroporous calcium phosphate bioceramics with nested chitosan sponges for load bearing bone implants. J Biomed Mater Res 2002;61:1–8.
[29] Lange FL, Miller KT. Open cell, low density ceramics fabricated from reticulated polymer substrates. Adv Ceram Mater 1987;2:827–31.
[30] Gibson LJ. The mechanical behavior of cancellous bone. Biomechanics 1985;18:317–28.
[31] LeGeros RZ, LeGeros JP, Daculsi G, Kijkowska R. Calcium phosphate biomaterials: preparation, properties, and biodegradation. In: Wise DL, Trantolo DJ, Altobelli DE, Yaszemski MJ, Gresser JD, Schwartz ER, editors. Encyclopaedia Hand book of Biomaterials and Bioengineering. Part A, vol. 2, no. 43. New York: Marcel Dekker; 1995. p. 1429–63.
[32] Hench LL, Wilson J. An introduction to bioceramics. London, UK: World Scientific; 1993.
[33] Rejda BV, Peelen JGJ, de Groot K. Tri calcium phosphate as bone substitute. J Bioeng 1977;1:93–7.
[34] Bleach NC, Tanner KE, Kellomaki M, Tormala P. Effect of filler type on the mechanical properties of self reinforced polylactide calcium phosphate composites. J Mater Sci Mater Med 2001;12:911–5.
[35] Callister WD. Materials science and engineering, an introduction, 6th ed. New York: Wiley; 2003.
[36] Porter NL, Pilliar RM, Gynpas MD. Fabrication of porous calcium polyphosphate implants by solid freeform fabrication: a study of processing parameters and in vitro degradation characteristics. J Biomed Mater Res 2001;56:504–15.
[37] Hollander W, den Patka, Klein PCPAT, Heidendal GAK. Macroporous calcium phosphate ceramics for bone substitution: a tracer study on biodegradation with ^{45}Ca Tracer. Biomaterials 1991;12:569–73.
[38] Frayssinet P, Trouillet JL, Rouquet N, Azimus E, Autefage A. Osseointegration of macroporous calcium phosphate ceramics having a different chemical composition. Biomaterials 1993;14:423–9.
[39] Yang X, Wang Z. Synthesis of biphasic ceramics of hydroxyapatite and β-tricalcium phosphate with controlled phase content and porosity. J Mater Chem 1998;8:2233–7.
[40] Kivrak N, Tas AC. Synthesis of calcium hydroxyapatite–tricalcium phosphate (HA–TCP) composite bioceramic powders and their sintering behavior. J Am Ceram Soc 1998;81:2245–52.
[41] Bauer TW, Muschler GF. Bone graft materials: an overview of the basic science. Clin Orthop 2000;371:10–27.
[42] Ducheyne P, Qiu Q. Bioactive ceramics: the effect of surface reactivity on bone formation and bone cell function. Biomaterials 1999;20:2287–303.
[43] Niihara K. New design concept of structural ceramics. Ceramic nano composites. J Ceram Soc Japan 1991;99:945–52.
[44] Liu Q, Gao L, Yan DS, Thompson DP. Hard silicon ceramics reinforced with SiC nanoparticles. Mater Sci Eng A—Struct Mater Prop Microstruct Process 1999;269:1–7.
[45] Cain M, Morrell R. Nanostructured ceramics: a review of their potential. Appl Organomet Chem 2001;15:321–30.
[46] Awaji H, Choi SM, Yagi E. Mechanisms of toughening and strengthening in ceramic-based nanocomposites. Mech Mater 2002;34:411–22.
[47] Liu DM. Densification of zirconia from submicron sized to nano sized powder particles. J Mater Sci Lett 1998;17:467–9.
[48] Provenzano V, Louat NP, Imam MA, Sadananda K. Ultrafine superstrength materials. Nanostructured Mater 1992;1:89–94.
[49] Ahn ES, Gleason NJ, Nakahira A, Ying JY. Nanostructure processing of hydroxyapatite based bioceramics. Nano Lett 2001;1:149–53.
[50] Cullity BD. X-ray diffraction. Reading, MA: Addison-Wesley; 1959.
[51] Higgins RJ, Rhine WE, Cima MJ, Bowen HK. Ceramic surface reactions and carbon retention during non oxidative binder removal: AL_2O_3/poly(methyl methacrylate) at 20–700°C. J Am Ceram Soc 1994;77:2243–53.
[52] Yan H, Cannon WR, Shanefield DJ. Evolution of carbon during burnout and sintering of tape cast aluminum nitride. J Am Ceram Soc 1993;76:166–72.
[53] Edirisinghe MJ. Binder removal from moulded ceramic bodies in different atmospheres. J Mater Sci Lett 1991;10:1338–41.
[54] Hwang KS, Huang HS. The liquid phase sintering of molybdenum with Ni and Cu additions. Mater Chem Phys 2001;67:92–100.
[55] Poirson A, Decorse P, Caboche G, Dufour LC. A dilatometeric study of the $La_{0.8}Sr_{0.2}MnO_3$ sintering behavior. Solid State Ionics 1997;99:287–95.
[56] Best S, Sim B, Kayser M, Downes S. Dependence of osteoblastic response on variations in the chemical composition and physical properties of hydroxyapatite. J Mater Sci Mater Med 1997;8:97–103.
[57] Eggli PS, Muller W, Schenk RK. Porous hydroxyapatite and tricalcium phosphate cylinders with two different pore size ranges implanted in the cancellous bone of rabbits. Clin Orthop Rel Res 1988;232:127–38.
[58] Famery R, Richard N, Boch P. Preparation of α- and β-tricalcium phosphate ceramics, with and without magnesium addition. Ceram Int 1994;20:327–36.
[59] Tampieri A, Celotti G, Szontagh F, Landi E. Sintering and characterization of HA and TCP bioceramics with control of their strength and phase purity. J Mater Sci Mater Med 1997;8:29–37.
[60] Wang PE, Chaki TK. Sintering behaviour and mechanical properties of hydroxyapatite and dicalcium phosphate. J Mater Sci Mater Med 1993;4:150–8.
[61] Boyde A, Corsi A, Quarto R, Cancedda R, Bianco P. Osteoconduction in large macroporous hydroxyapatite ceramic implants: evidence for a complementary integration and disintegration mechanism. Bone 1999;6:579–89.
[62] Atahanasiou KA, Zhu CF, Lanctot, Agrawal CM, Wang X. Fundamentals of biomechanics in tissue engineering of bone. Tissue Eng 2000;6:361–81.
[63] Luo J, Stevens R. The role of residual stress on the mechanical properties of Al_2O_3 5 vol% SiC nano composites. J Eur Ceram Soc 1997;17:1565–72.
[64] Ohji T, Jeong YK, Choa YH, Niihara K. Strengthening and toughening mechanisms of ceramic nanocomposites. J Am Ceram Soc 1998;81:1453–60.
[65] Li WQ, Gao L. Processing, microstructure and mechanical properties of 25 vol% YAG-Al_2O_3 nanocomposite. Nanostructured Mater 1999;11:1073–80.
[66] Kovalev S, Ohji T, Yamauchi Y, Sakai M. Grain boundary strength in non cubic ceramic polycrystals with misfitting intragranular inclusions (nanocomposites). J Mater Sci 2000;35:1405–12.
[67] Li G, Jiang A, Zhang L. Mechanical and fracture properties of nano Al_2O_3 alumina. J Mater Sci Lett 1996;15:1713–5.
[68] Nakamura S, Otsuka R. Thermal expansion of hydroxyapatite-β-tricalcium phosphate ceramics. Termochim Acta 1990;165:57–72.

[69] Jiao S, Jenkins ML, Davidge RW. Processing and fracture toughness of nano sized Cu dispersed Al_2O_3 composites. Acta Metall 1997;45:149–56.

[70] Pezzotti G, Sakai M. Effect of silicon carbide Nano dispersion on the mechanical properties of silicon nitride. J Am Ceram Soc 1994;77:3039–41.

[71] Hoffman1 M, Rodel Jurgen. Suggestion for mechanism of strengthening of nanotoughened ceramics. J Ceram Soc Japan 1997;105:1173–8.

[72] Rouxel T, Wakai F, Brito ME, Iwamoto A, Izaki K. Intragranular crack deflection and crystallographic slip in Si_3N_4/SiC nano composites. J Eur Ceram Soc 1993;11:431–8.